24th COBEM - 2017

24th ABCM International Congress of Mechanical Engineering
December 3-8, 2017, Curitiba, PR, Brazil

COBEM-2017-0881
ROBUST DESIGN AND UNCERTAINTY ANALYSIS OF AN ENERGY HARVESTING RESONANT DEVICE

Paulo Henrique Martins
Marcelo Areias Trindade
Department of Mechanical Engineering, São Carlos School of Engineering, University of São Paulo, São Carlos, SP 13566-590, Brazil
paulo.martins@usp.br, trindade@sc.usp.br

Abstract. *The use of electrical energy increases continuously and very rapidly and, thus, the search for alternative energy sources attracts important research effort. Recently, several studies were directed to energy harvesting from ambient sources, such as mechanical vibrations from machines and structures. One popular energy harvesting device consists on a cantilever beam with tip mass, designed to resonate at the operating frequency of the machine to which it is attached. The beam bending vibration is then converted into electrical energy through a bonded piezoelectric material that should be connected to a proper harvesting circuit. To ensure greater amounts of harvested energy, it is important to optimize the harvesting device as well as properly tune resonance and operating frequencies. Besides, even optimized devices performance may be affected by uncertainties and variabilities due to environmental changes and/or manufacturing tolerances. Therefore, robust design techniques may be required in order to reduce device's performance sensitivity to expected uncertainties. There exists some well-known robust design optimization techniques, but there is not much research applying them to dynamics and vibrations since it may be computationally expensive. This work aims at applying a less expensive robust design technique, known as Taguchi method, to design a piezoelectric energy harvesting device when subjected to uncertainties in harvesting circuit impedance, device-machine attachment effectiveness, and overall damping. This is done using an electromechanical coupled finite element model for the cantilever beam with tip mass and base excitation. Deterministic Sequential Quadratic Programming optimization is performed to guarantee proper tuning of nominal harvesting devices. Then, using Taguchi method, a search for devices and circuit impedance that provide satisfactory trade-off between nominal performance and robustness is performed. Results show that with little deviation from nominal designs, robustness can be increased without much loss in mean performance.*

Keywords: *Energy harvesting, uncertainties, vibration, robust design, piezoelectric materials*

1. INTRODUCTION

The use of electrical energy increases continuously and very rapidly and, thus, the search for alternative energy sources which may ensure economy and/or allow energy reuse or harvesting from ambient sources has been attracting important research effort is the past decades. In several cases, an important part of operation energy is wasted in equipments through heat, noise and vibration. Hence, a rapidly growing research effort has been directed to techniques that allow to collect this wasted energy and transform it into usable energy. Some examples involve harvesting usable energy from thermal sources, wind power, light sources, motion and chemical reactions. In particular, through their electromechanical coupling properties, piezoelectric materials are a class of so-called smart or intelligent or functional materials, that are able to convert strain energy into electrical energy since when their internal electric dipoles are deformed electrical charges appear. The amount of converted energy naturally depends on the strain energy available but also on piezoelectric material and geometric properties (Leo, 2007).

Piezoelectric materials can be used in foot wears, dance floors, airport runways, vehicles or bridges to convert the mechanical energy of motion into electricity (Kalyani *et al.*, 2015). Most piezoelectric energy harvesting devices consists of resonant cantilever beams (substrate), with a seismic mass attached to their free end, covered with piezoelectric layers (sensors) that are connected to electric circuits, as shown in Fig. 1. The beam clamp is supposed to move rigidly with the equipment (base) to which the device is attached . Through base excitation, the device vibrates and allows the conversion of mechanical energy into electricity thanks to the piezoelectric sensors and electric circuits. The generated energy can be used to power portable devices or sensors as well as wider range of sources (Erturk and Inman, 2011).

Figure 1 shows an example of a cantilever beam device used in energy harvesting. The device is excited by the displacement $\mathrm{w(t)}$ in the support and is composed of beam (substrate) with length L, seismic mass $\mathrm{M_t}$ and electric circuit with resistance R (shunt circuit), which allows to measure a voltage output $\mathrm{v(t)}$ between electrodes of piezoceramic sensor and beam (substrate). The piezoceramic with electrodes covers all the substrate and a poling direction scheme as

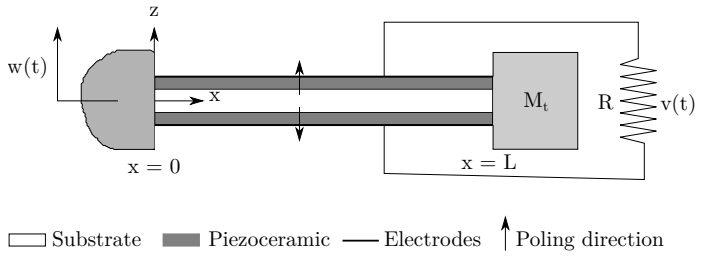

Figure 1. Typical device model for energy harvesting (Erturk and Inman, 2011)

shown in Fig. 1 is assumed (Ramadan *et al.*, 2014).

To improve the efficiency of resonant harvesting devices, it is important to tune the operation and resonance frequencies using seismic masses to increase the vibration amplitude. The available energy to be converted into electricity is generally small and, thus, sophisticated designs may be required to increase the efficiency. The structural performance can be improved by using optimization techniques which generate designs with better performing geometries.

Generally speaking, optimization processes search for design parameters that lead to maximum or minimum values of a cost function considering a number constraints. A classic deterministic optimization problem subject to constraints can be written as

$$\begin{aligned} \text{optimize} \quad & f(\mathbf{x}) \\ \text{subject to} \quad & g_i(\mathbf{x}) \leq 0 \quad i = 1, 2, \cdots, I \\ & s_j(\mathbf{x}) = 0 \quad i = 1, 2, \cdots, J \end{aligned} \tag{1}$$

where $\mathbf{x}$ is the vector of design parameters, $g_i(\mathbf{x})$ represents the inequality constraints and $s_j(\mathbf{x})$ equality constraints.

There are many well-known optimization techniques considering cost functions that can be quadratic, geometric, linear and nonlinear (Rao, 2009). Dealing with nonlinear cost functions may be difficult in some situations and an important algorithm is the Sequential Quadratic Programming (SQP) which change the nonlinear problem into a quadratic problem that can be easily solved.

Standard optimization techniques find optimum solutions in deterministic problems, but when uncertainties are considered other techniques are necessary. Robust Design Optimization (RBO) or Robust Design can be used since it considers the uncertainties in the problems and verifies the sensitivity of the designs with respect to these uncertainties (Schuëller and Jensen, 2008). When environmental variations (temperature, pressure, humidity, vibrations, etc) happen, the design can be affected as well as through manufacturing process, deterioration and ineffective assemblies. In this situation, robust design techniques may be used and the optimum solution generally is different from the one obtained using deterministic optimizations. Robust designs consider the design variables and uncertainties in the analysis then Eq. (1) is modified and constraints may also have uncertainties.

To understand robust design optimization, Fig. 2 presents target solutions (larger black circle) to be found. The smaller black circles in Fig. 2 represent problem variation. Then, through optimization methods the target is found, but variability may be high as shown in Fig. 2b. The case shown in Fig. 2d is better because the solution is on target and there is low variability. In others cases, the target solution is not found with either low (Fig. 2a) or high (Fig. 2c) variability.

In the 1960s, Genichi Taguchi developed a methodology to improve the productivity in companies considering the robust design concept. Usually, there is variability in products and the optimum solutions must be changed. Then, Taguchi considered the variability or uncertainties as well as environmental variations in processes as noises and developed a methodology to guarantee that products are less affected by these noises. The methodology is based on control factors or variables that are controllable and noise factors which are uncontrollable environmental variations or uncertainties in materials, processes, assemblies, etc. To increase robustness, the technique chooses control factors that make the product less sensitive to sources of variability.

2. CLAMPED BEAM MODEL FOR ENERGY HARVESTING

To evaluate the energy harvested in devices, a development is performed based on a finite element model for a sandwich beam with piezoelectric layers proposed in (Santos, 2008). The model was developed considering Bernoulli-Euler and Timoshenko theories for beam surface layers and core, respectively. Furthermore, orthotropic piezoelectric material was assumed in plane stress state and perfectly bonded. The model includes two nodes per finite element with four mechanical and three electrical degrees of freedom per node. In the present study, only top surface layer is considered to be piezoelectric which is assumed transversely poled. The electric circuit, to which the piezoelectric layer is connected, is

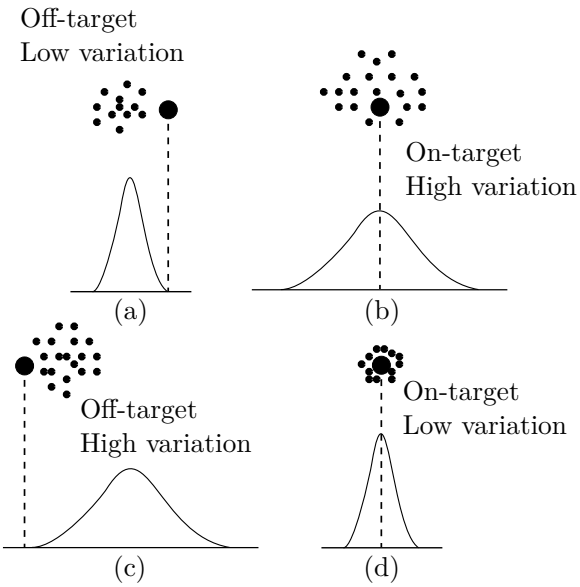

Figure 2. Target solution and variation in problems (Zang *et al.*, 2005)

composed of an electric resistance to represent the harvesting circuit impedance. These model assumptions and procedures lead to the following set of equations of motion

$$\begin{bmatrix} \boldsymbol{M} & 0 \\ 0 & 0 \end{bmatrix} \begin{Bmatrix} \ddot{\boldsymbol{u}} \\ \ddot{\boldsymbol{q}}_c \end{Bmatrix} + \begin{bmatrix} 0 & 0 \\ 0 & \boldsymbol{R}_c \end{bmatrix} \begin{Bmatrix} \dot{\boldsymbol{u}} \\ \dot{\boldsymbol{q}}_c \end{Bmatrix} + \begin{bmatrix} \boldsymbol{K}_m & -\bar{\boldsymbol{K}}_{me} \\ -\bar{\boldsymbol{K}}_{me}^t & \bar{\boldsymbol{K}}_e \end{bmatrix} \begin{Bmatrix} \boldsymbol{u} \\ \boldsymbol{q}_c \end{Bmatrix} = \begin{Bmatrix} \boldsymbol{F} \\ 0 \end{Bmatrix} \tag{2}$$

where $\boldsymbol{M}$ is the mass matrix of system, $\boldsymbol{R}_c$ the electrical resistance matrix, $\boldsymbol{K}_m$ the mechanical stiffness matrix, $\bar{\boldsymbol{K}}_{me}$ the piezoelectric stiffness matrix and $\bar{\boldsymbol{K}}_e$ the dielectric stiffness matrix. $\boldsymbol{F}$, $\boldsymbol{q}_c$ and $\boldsymbol{u}$ are representative vectors for external forces, circuit electric charges and global mechanical displacements, respectively.

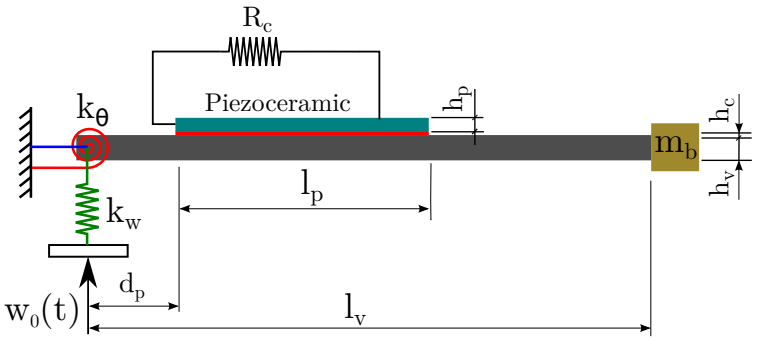

Figure 3. Beam model for energy harvesting study

The energy harvesting device considered in the present study, schematically represented in Fig. 3, is composed of beam (substrate), piezoceramic , adhesive layer (red), seismic mass m_b, shunt circuit with electrical resistance R_c and device clamp with torsional and linear stiffness k_θ and k_w, respectively. The dimensions of device are summarized as follow; beam length: l_v; beam height: h_v; piezoceramic height: h_p; adhesive layer height: h_c; piezoceramic and adhesive layers length: l_p; piezoceramic and adhesive layers distance from clamp: d_p. When a harmonic displacement $w_0(t)$ is prescribed at the clamp, it is possible to estimate the harvestable energy from this excitation by means of the energy dissipated in the electrical resistance R_c using the proposed finite element.

The mechanical stiffness and mass matrices of Eq. (2) are modified to account for the springs stiffnesses in clamp and seismic mass at the free end of the cantilever beam. In addition, due to the harmonic base excitation $w_0(t)$ an equivalent force due to the clamping stiffness is applied to the cantilever beam. This can be observed by including the prescribed displacement to the model, such that

$$\begin{bmatrix}\delta w_0 & \boldsymbol{\delta u}_r^t\end{bmatrix}\left\{\begin{bmatrix}M_{pp} & \boldsymbol{M}_{pr}\\ \boldsymbol{M}_{pr}^t & \boldsymbol{M}_{rr}\end{bmatrix}\begin{bmatrix}\ddot{w}_0\\ \ddot{\boldsymbol{u}}_r\end{bmatrix}+\begin{bmatrix}K_{pp} & \boldsymbol{K}_{pr}\\ \boldsymbol{K}_{pr}^t & \boldsymbol{K}_{rr}\end{bmatrix}\begin{bmatrix}w_0\\ \boldsymbol{u}_r\end{bmatrix}-\begin{bmatrix}0\\ 0\end{bmatrix}\right\}=0 \tag{3}$$

where subscript "p" represents the degrees of freedom which are prescribed and other degrees of freedom are represented by subscript "r". The displacement w_0 is known then δw_0 is zero and Eq. (3) is simply reduced to

$$\boldsymbol{M}_{rr}\ddot{\boldsymbol{u}}_r+\boldsymbol{K}_{rr}\boldsymbol{u}_r=-\boldsymbol{M}_{pr}^t\ddot{w}_0-\boldsymbol{K}_{pr}^t w_0 \tag{4}$$

Mass elements are not present at the clamp then $\boldsymbol{M}_{pr}^t$ is zero and Eq. (4) becomes:

$$\boldsymbol{M}_{rr}\ddot{\boldsymbol{u}}_r+\boldsymbol{K}_{rr}\boldsymbol{u}_r=-\boldsymbol{K}_{pr}^t w_0 \tag{5}$$

where $\boldsymbol{M}_{rr}$ is the mass matrix modified due to the seismic mass at the free end of the cantilever beam and $\boldsymbol{K}_{rr}$ is the mechanical stiffness matrix modified due to springs in the clamp. The spring linear forces in device are represented by $\boldsymbol{F}_p=-\boldsymbol{K}_{pr}^t w_0$ in Eq. (5) and the matrix $\boldsymbol{K}_{pr}^t$ refers to spring elements in the corresponding degree of freedom. One linear spring is at the clamp then the first mechanical degree of freedom is influenced by a linear spring force

$$f_p=k_w w_0 \tag{6}$$

Then, Eq. (2) can be modified and expressed as

$$\begin{bmatrix}\boldsymbol{M}_{rr} & 0\\ 0 & 0\end{bmatrix}\begin{Bmatrix}\ddot{\boldsymbol{u}}\\ \ddot{\boldsymbol{q}}_c\end{Bmatrix}+\begin{bmatrix}0 & 0\\ 0 & \boldsymbol{R}_c\end{bmatrix}\begin{Bmatrix}\dot{\boldsymbol{u}}\\ \dot{\boldsymbol{q}}_c\end{Bmatrix}+\begin{bmatrix}\boldsymbol{K}_{rr} & -\bar{\boldsymbol{K}}_{me}\\ -\bar{\boldsymbol{K}}_{me}^t & \bar{\boldsymbol{K}}_e\end{bmatrix}\begin{Bmatrix}\boldsymbol{u}\\ \boldsymbol{q}_c\end{Bmatrix}=\begin{Bmatrix}\boldsymbol{F}_p\\ 0\end{Bmatrix} \tag{7}$$

Then, the device model represented by Eq. (7) is used to evaluate the frequency response function (FRF) for harvestable power output and base acceleration input, considering one piezoelectric material bonded to the substrate and connected to an electric resistance. The spring forces can be written as $\boldsymbol{F}_p=\boldsymbol{b}f_p(t)$ where $\boldsymbol{b}$ is a column vector that defines the position of spring force and $f_p(t)=\tilde{f}_p e^{j\omega t}$. Considering the nodal displacements projected onto a truncated undamped modal basis such that $\boldsymbol{u}=\boldsymbol{\phi}\boldsymbol{\alpha}$, the FRF can be evaluated as shown in (Trindade *et al.*, 2013). For that, modal projections of the system matrices and vectors are defined as $\boldsymbol{I}=\boldsymbol{\phi}^t\boldsymbol{M}_{rr}\boldsymbol{\phi}$, $\boldsymbol{\Omega}^2=\boldsymbol{\phi}^t\boldsymbol{K}_{rr}\boldsymbol{\phi}$, $\boldsymbol{K}_p=\boldsymbol{\phi}^t\bar{\boldsymbol{K}}_{me}$ and $\boldsymbol{b}_\phi=\phi^t\boldsymbol{b}$. Then, starting from harmonic base displacement input $w_0(t)=\tilde{w}_0 e^{j\omega t}$ and harmonic electric charge output $q_c(t)=\tilde{q}_c e^{j\omega t}$, leading to an also harmonic electric current with amplitude $\tilde{I}=j\omega\tilde{q}_c$, it is possible to define the FRF between electric current output and base displacement input as

$$G_{Iw}(\omega)=j\omega k_w\boldsymbol{K}_p^t[\boldsymbol{D}^{-1}]\boldsymbol{b}_\phi \tag{8}$$

where $[\boldsymbol{D}]=[(j\omega R_c+\bar{K}_e)(-\boldsymbol{I}\omega^2+j2\omega\boldsymbol{\Lambda}\boldsymbol{\Omega}+\boldsymbol{\Omega}^2)-\boldsymbol{K}_p\boldsymbol{K}_p^t]$ and $\boldsymbol{\Lambda}$ is the modal damping matrix for the system.

The FRF for power output can be found considering $\tilde{P}=R_c\tilde{I}^2$. Then, FRF power output by squared displacement input $G_{Pw}(\omega)$ can be written as

$$G_{Pw}(\omega)=R_c G_{Iw}(\omega)^2 \tag{9}$$

Considering that base displacement amplitude times the squared frequency yields base acceleration amplitude, it is possible to deduce the FRF for power output by squared acceleration input G_{Pa} as

$$G_{Pa}(\omega)=(1/\omega^4)G_{Pw}(\omega) \tag{10}$$

In the present work, high values of the Eq. (10) represent an increase in energy harvested. Furthermore, tuning the operation frequency at the clamp and resonant frequency of device is essential.

3. OPTIMIZATION WITH ORTHOGONAL ARRAYS

The Taguchi method is based on orthogonal arrays which are special matrices with many experiments to evaluate the response signal considering the control factors and noise factors. The methodology verifies the difference between target and actual response and choose control factors to minimize the deviation considering noises in the process. Furthermore, Taguchi introduced a relation named signal-to-noise (S/N) to evaluate the design sensibility and final robustness. Through orthogonal arrays, it is possible to calculate mean, variance and signal-to-noise for many experiments and perform an analysis of variance (ANOVA) to obtain a robust design (Zang *et al.*, 2005).

The signal-to-noise (S/N) may be used for different types of problems and larger values of S/N for a given design means robustness increase. The standard types of problems considered are larger-the-better (LB), smaller-the-better (SB), nominal-the-best (NB) and signed-target (ST). The larger-the-better and smaller-the-better relations are used to determine proper control factors that, respectively, maximize and minimize the cost function. When target values are known, the nominal-the-best and signed-target relations are appropriated, where the latter is considered for null targets (Phadke, 1995). Table 1 presents the standard types of problems with range for observations, ideal values and S/N ratios.

Table 1. Problems types and S/N ratio (Phadke, 1995)

Problem type	Range	Ideal value	S/N Ratio
Smaller-the-better (SB)	$0 \leq y \leq \infty$	0	$S/N = -10\log_{10}\left(\frac{1}{n}\sum_{i=1}^{n} y_i^2\right)$
Nominal-the-best (NB)	$0 \leq y \leq \infty$	nonzero, finite	$S/N = 10\log_{10}(\mu^2/\sigma^2)$
Larger-the-better (LB)	$0 \leq y \leq \infty$	∞	$S/N = -10\log_{10}\left(\frac{1}{n}\sum_{i=1}^{n} 1/y_i^2\right)$
Signed-target (ST)	$-\infty \leq y \leq \infty$	finite, usually 0	$S/N = -10\log_{10}\sigma^2$

Table 1 presents standard deviation (σ), mean (μ) and functions analyzed (y_i) into S/N ratio. The zero value is generally a target in signed-target problems but it is possible change to the reference value. Then, nominal-the-best and signed-target problems types can be studied similarly. In LB and SB, the maximum or minimum values for function are found to determine control factors, but in NB and ST it is necessary to adjust or scale factors to find the target values. This methodology does not have constraints with uncertainties differently of some classics methods for robust design. An alternative is to optimize the problem deterministically finding the target value and, then, to apply Taguchi method (Park *et al.*, 2006). Furthermore, the analysis is divided in two steps: first, the variance is decreased and after this (second step) the mean is changed to the target. When S/N ratio is maximized, the variance decreases (first step) and by finding a control factor that does not influence the S/N ratio, it is possible to change the mean to the target. This control factor is named adjustment or scale factor but in some cases, it is difficult to find an adjustment factor. Therefore, optimizing the problem deterministically is important because it makes possible to choose control factors near the optimum value.

To evaluate the S/N ratio, it is necessary to properly choose the orthogonal arrays. There are many available arrays in the literature according to control factors or noise factors numbers and levels. The process of choosing an array is based on degrees of freedom of problem that have to be smaller or equal to matrix lines. Usually, the number of degrees of freedom associated with factors is equal to the number of levels minus one and with the mean is equal to one. Therefore, the sum of these degrees of freedom is the total numbers of degrees of freedom in a problem. The matrices for control factors and noise factors are named inner array and outer array, respectively (Phadke, 1995).

After calculating the S/N ratio, mean and variance through orthogonal arrays, it is possible to evaluate the effect of the control factors associated with the response.

4. METHODOLOGY

In this section, the proposed methodology is presented aiming at designing an energy harvesting device that maximizes the harvesting performance, defined as the harvested power per squared base acceleration as in Eq. (10) for a given excitation frequency, but, at the same time, maximizes its robustness when subjected to uncertainties in clamp stiffness, electrical resistance and damping. First, a deterministic optimization, using SQP, is performed to find optimal devices under design constraints. Then, robust optimization, using orthogonal arrays, is performed to evaluate the robustness of each optimal device.

4.1 Device Optimization

The optimization is performed using SQP algorithm in Matlab® to find optimum dimensions for the device. Some parameters are predetermined as follows: distance from the clamp d_p, piezoceramic height h_p, beam height h_v and adhesive layer height h_c. The piezoceramic length is considered 80% of the beam length and vector $\mathbf{x}_p = [l_v, m_b, R_c]$ is

defined to optimize or to find the peak in Eq. (10). Then, considering $f(\mathbf{x}_p) = G_{Pa}(\omega)$, it is possible to write

$$\begin{aligned} &\text{maximize} && f(\mathbf{x}_p) \\ &\text{subject to} && l_{vl} \leq l_v \leq l_{vu} \\ & && m_{pl} \leq m_b \leq m_{pu} \end{aligned} \tag{11}$$

where subscripts l and u represent lower and upper bounds, respectively. The maximum value of $f(\mathbf{x}_p)$ for given constraints is defined as the optimal solution and its parameters are separated to constitute the device parameters. In optimization, the resonant frequency and operation frequency are tuned because the peak of Eq. (10) is in resonant frequency. The optimal devices are, then, automatically tuned to output maximum harvested power at the pre-defined operation frequency.

4.2 Robust Analysis

With the optimum devices, robust analysis are made to verify the sensitivity to uncertainties in springs, electric resistance and damping. To make robust analysis through Taguchi method, it is necessary to separate control factors and noise factors. Applying the technique allows to find variance, mean and signal-to-noise for FRF power output in Eq. (10). For each design, there is one seismic mass and beam length appropriate for frequency tuning. The electric resistance will change the frequency a little if the select points are close to the optimum. Therefore, seismic mass and electrical resistance might be the control factors whereas clamp stiffness and damping the noise factors. Thus, the control factors are written in vector form $\boldsymbol{x}$ as shown below

$$\boldsymbol{x} = [m_b, R_c] \tag{12}$$

The noise factors can be written in vector form $\boldsymbol{z}$ and is shown in Eq. (13) below where ζ is the damping factor.

$$\boldsymbol{z} = [k_w, k_\theta, \zeta] \tag{13}$$

The response signal or power output is influenced by the noise factors and can be controlled by the control factors. Considering the function $\boldsymbol{g} = (\boldsymbol{x}, \boldsymbol{z})$, the diagram with control factors and noise factors inputs as well as response signal is shown below in Fig. 4.

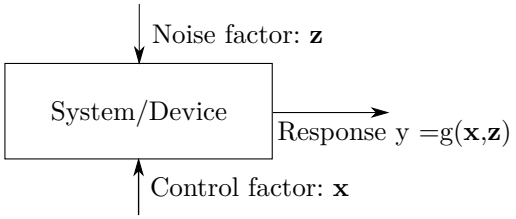

Figure 4. Diagram with inputs and output in the system

In the present work, there are control and noise factors, then inner and outer arrays are utilized. The electric resistance is a control factor considered with tolerance, then inner and outer array are utilized simultaneously to this factor. The proper inner array might have two columns because there are two factors ($R_c,\ m_b$) while outer array must have four columns for factors ($k_w,\ k_\theta,\ \zeta,\ R_c$). Considering the noise factors with normal distribution and with tolerance defined by three standard deviations, two levels might be written for each noise factor. The levels refer to limits for each noise factor in the normal distribution chart. For five devices with ten electrical resistances to choose, an inner array with five levels for devices and ten levels for electrical resistances are required. Then, one inner array $L_8(2^7)$ and outer array $L_{50}(2^1 \times 5^{11})$ can be utilized. The representation $L_N(s^m)$ means that there are N rows, m columns and s levels in inner array or outer array. There are one column with two levels and eleven with five levels in inner array, but electric resistance requires ten levels. Then, inner array have to be modified and the first two columns are merged to make one ten level column. In (Phadke, 1995) the matrix $L_8(2^7)$ is modified to make one column with four levels and many matrices types are presented for studies. The Tab. 2 presents the orthogonal array $L_8(2^7)$ and the modified array with four levels in the first column. Then, inner array $L_{50}(2^1 \times 5^{11})$ can be modified similarly to find the columns with ten and five levels.

After deterministic optimization procedure, each device is designed to deliver the maximum power for a given electric resistance. Then, in a second step, the electrical resistance that maximizes the harvested power can be evaluated. For robust design, electrical resistance is considered also as a noise factor, that is subjected to variability, and, thus, it is varied around its optimum value. The maximum power is, then, defined as the target value for each device design. The signed-target problem is utilized to verify the sensitivity with noise factors. The maximum power for each device is considered

Table 2. $L_8(2^7)$ Orthogonal array and array modified with four leves in the first column

Exp.	c1	c2	c3	c4	c5	c6	c7
1	1	1	1	1	1	1	1
2	1	1	1	2	2	2	2
3	1	2	2	1	1	2	2
4	1	2	2	2	2	1	1
5	2	1	2	1	2	1	2
6	2	1	2	2	1	2	1
7	2	2	1	1	2	2	1
8	2	2	1	2	1	1	2

Exp.	c1 x c2	c4	c5	c6	c7
1	1	1	1	1	1
2	1	2	2	2	2
3	2	1	1	2	2
4	2	2	2	1	1
5	3	1	2	1	2
6	3	2	1	2	1
7	4	1	2	2	1
8	4	2	1	1	2

as a reference in target problem. Then, mean, variance and S/N are studied to choose a robust device and to verify the mean (power generated). For example, the inner and outer array are shown in Tab. 3 with control and noises factors in appropriate columns. The noise factors are into the first four columns in $L_8(2^7)$ and control factors into the two first columns in orthogonal array $L_8(2^7)$ modified. Thus, the responses are found in each row of orthogonal array $L_8(2^7)$ modified and the experiment responses y are about power generated. For this work, inner array is composed of ten levels in the first column and five in the second, but the outer array is $L_8(2^7)$.

Table 3. inner and outer array associated

		Exp.	1	2	3	4	5	6	7	8			
		k_w	1	1	1	1	2	2	2	2			
		k_θ	1	1	2	2	1	1	2	2			
		ζ	1	1	2	2	2	2	1	1			
		R_c	1	2	1	2	1	2	1	2			
Exp.	R_c	m_b	1	2	3	4	5	6	7	8			
1	1	1	y_{11}	y_{12}	y_{13}	y_{14}	y_{15}	y_{16}	y_{17}	y_{18}	$\mapsto \mu_1$	σ_1^2	S/N_1
2	1	2	y_{21}	y_{22}	y_{23}	y_{24}	y_{25}	y_{26}	y_{27}	y_{28}	$\mapsto \mu_2$	σ_2^2	S/N_2
3	2	1	y_{31}	y_{32}	y_{33}	y_{34}	y_{35}	y_{36}	y_{37}	y_{38}	$\mapsto \mu_3$	σ_3^2	S/N_3
4	2	2	y_{41}	y_{42}	y_{43}	y_{44}	y_{45}	y_{46}	y_{47}	y_{48}	$\mapsto \mu_4$	σ_4^2	S/N_4
5	3	1	y_{51}	y_{52}	y_{53}	y_{54}	y_{45}	y_{46}	y_{57}	y_{58}	$\mapsto \mu_5$	σ_5^2	S/N_5
6	3	2	y_{61}	y_{62}	y_{63}	y_{64}	y_{65}	y_{66}	y_{67}	y_{68}	$\mapsto \mu_6$	σ_6^2	S/N_6
7	4	1	y_{71}	y_{72}	y_{73}	y_{74}	y_{75}	y_{76}	y_{77}	y_{78}	$\mapsto \mu_7$	σ_7^2	S/N_7
8	4	2	y_{81}	y_{82}	y_{83}	y_{84}	y_{85}	y_{86}	y_{87}	y_{88}	$\mapsto \mu_8$	σ_8^2	S/N_8

The signal-to-noise (S/N) responses in orthogonal arrays experiments are used to calculate the effects and to verify the contribution of each control factors. The effects can be calculate through Eq. (14) which refer to the matrix $L_8(2^7)$.

$$\hat{R}_{c1} = (S/N_1 + S/N_2)/2, \quad \hat{R}_{c2} = (S/N_3 + S/N_4)/2, \quad \hat{R}_{c3} = (S/N_5 + S/N_6)/2, \quad \hat{R}_{c4} = (S/N_7 + S/N_8)/2,$$
$$\hat{m}_{b1} = (S/N_1 + S/N_3 + S/N_5 + S/N_7)/4, \quad \hat{m}_{b2} = (S/N_2 + S/N_4 + S/N_6 + S/N_8)/4. \tag{14}$$

where the hat is referent to the effect for each control factor level.

5. RESULTS

Firstly, the devices properties were defined for the parametric analysis, optimization and robust design. The beam was considered as aluminum and piezoelectric material is Lead Zirconate Titanate (PIC-151). The devices parameters are summarized as: distance from the clamp $5\ mm$, piezoceramic height $0.25\ mm$, beam height $1\ mm$ and adhesive layer height $0.1\ mm$, all with width of $25\ mm$. For the piezoelectric material, the properties are: elastic stiffness constant $\bar{c}_{11}^D = 101.24\ GPa$, piezoelectric coupling constant $\bar{h}_{31} = -1.4862 \times 10^9\ NC^{-1}$, dielectric constant $\bar{\beta}_{33}^\epsilon = 76.435 \times 10^6\ mF^{-1}$ and shear correction factor $k_2 = 0.83$. The Young's modulus $70\ GPa$ and density $2700kg\ m^{-3}$ is related to aluminum. The adhesive layer properties are: density $1126\ kg\ m^{-3}$ and Young's modulus $2.5\ GPa$ (Santos, 2012).

A nominal viscous damping for the system of $0.3\ \%$ was considered. The base acceleration input was considered as $a_c = g = 10\ m\ s^{-2}$ and with frequency of $100\ Hz$.

5.1 Optimization

The optimization process was realized to find five optimum devices which were separated in length of a bounded interval. A single bounded interval was considered for the seismic mass and for each device a different resistance was considered. Table 4 shows the five intervals for length and seismic mass with specific resistance.

Table 4. Bounded intervals and optimized parameters

	length (mm)	seismic mass (g)	resistance	$l_v\ (mm)$	$m_b\ (g)$	$R_c\ (\Omega)$
device 1	$50 \leq l_{v1} \leq 55$	$3 \leq m_{p1} \leq 45$	R_{c1}	50	13.978	214981
device 2	$55 \leq l_{v2} \leq 60$	$3 \leq m_{p2} \leq 45$	R_{c2}	55	10.386	206906
device 3	$60 \leq l_{v1} \leq 65$	$3 \leq m_{p1} \leq 45$	R_{c1}	60	7.782	201641
device 4	$65 \leq l_{v2} \leq 70$	$3 \leq m_{p2} \leq 45$	R_{c2}	65	5.837	184572
device 5	$70 \leq l_{v1} \leq 75$	$3 \leq m_{p1} \leq 45$	R_{c1}	70	4.342	179428

The intervals were divided in five points for length and mass and all combinations were used as initial guess in SQP algorithm. After optimization, the results for five devices can be shown in Tab. 4. Considering the following analysis, the electrical resistances for device 1 to device 5 were rounded to: 215, 210, 200, 185 and 180 $k\Omega$, respectively. For all optimum devices, the resonant frequency matches the operation frequency (100 Hz). For all optimum devices, the resonant frequency matches the operation frequency (100 Hz). Figs. 5a and 5b show the FRF amplitudes of voltage and power outputs and base acceleration input for the five optimum devices.

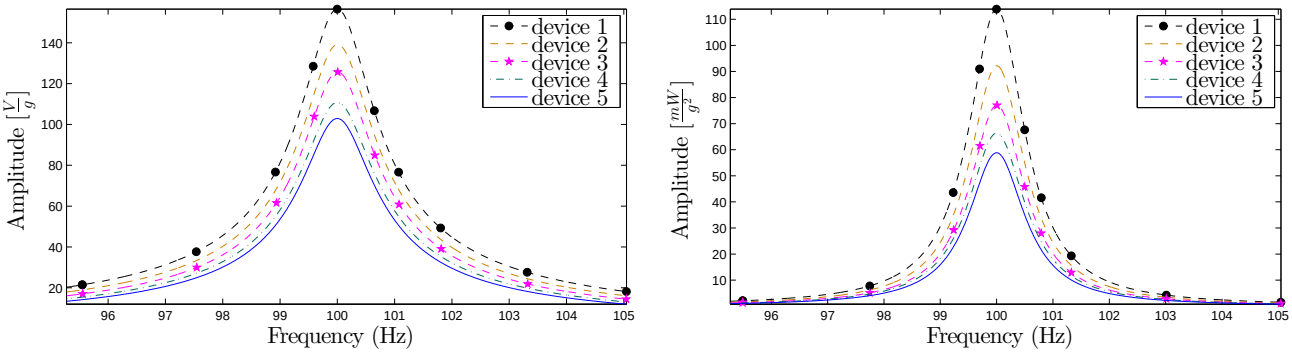

(a) FRF Voltage (b) FRF Power

Figure 5. FRF voltage and power for acceleration input

5.2 Robust Analysis

The robust analysis was based on uncertainties in clamp stiffness, damping and electrical resistance. Figures 6a and 6b were plotted to verify the variation of the voltage output with the stiffness at the clamp. It can be observed in Fig. 6 that from 3000 kNm^{-1} for linear stiffness and 5 $kNm\ rad^{-1}$ for torsional stiffness, the amplitude of voltage output converges to its maximum. Therefore, these values were used as nominal values to calculate the sensitivity of the performance to variabilities in these stiffnesses, aiming at representing imperfect clamping. Furthermore, tolerances of 50% were supposed for each spring considering three standard deviation while for the damping, a tolerance of 10% was considered.

Concerning electrical resistance, the optimum values with the SQP algorithm were chosen as nominal values for the devices, but a tolerance of 2% was considered. Furthermore, other five resistances values were chosen to compare the response. Figure 7 shows the power in terms of the resistance. It is noticeable that power does not change too much, then several of the considered resistance values near the optimum (215, 210, 200, 185 and 180 $k\Omega$) yield very satisfactory harvesting performance. Additional values were chosen as 120, 140, 160, 240 and 260 $k\Omega$ to verify the sensitivity.

After determining the devices with control factors (m_b and R_c) and noise factors (k_w, k_θ and ζ), the Taguchi method was applied. For each combination between devices and resistances, specific values of mean, variance and S/N may be evaluated. From this, effects for factors were calculated as displayed in Fig. 8. It is important that S/N increase, then low

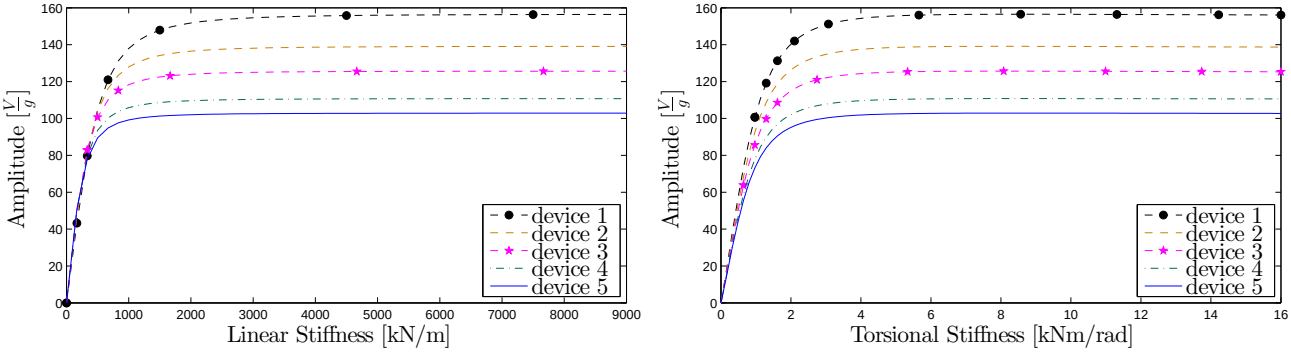

(a) Linear Stiffness (b) Torsional Stiffness

Figure 6. Voltage output versus linear and torsion stiffness at the clamp for acceleration input

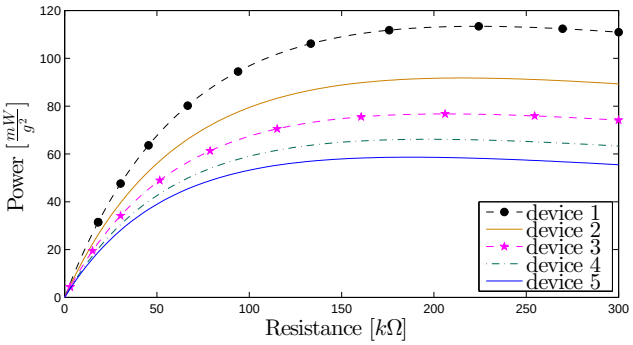

Figure 7. Power output versus resistance

resistances are better for that though mean value decreases a little. Then, low resistances near the optimum are important to decrease the variability in response and increase the resistance is not suitable. A comparison between the values in mean (red chart) and sensitivity (blue chart) shows that the first device is better to generate energy while the fifth is more robust.

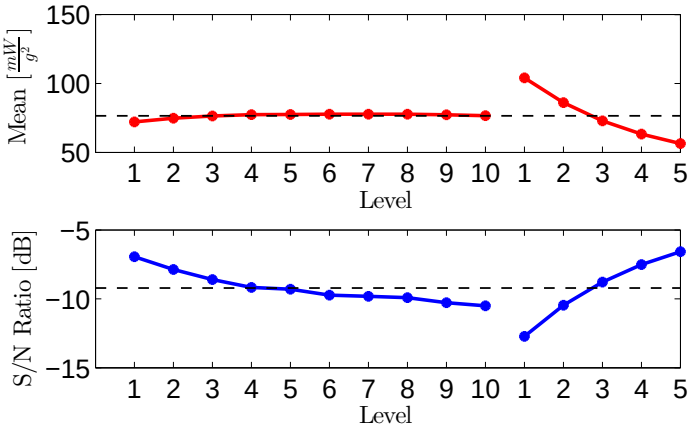

Figure 8. Factors effect on FRF power

For each device with optimal (deterministic cases) and smallest resistances (robust cases), the bar charts were plotted as shown in Figs. 9a and 9b. With the optimal resistances, the first device generates more energy $(107.38 \pm 13.58) mW\ g^{-2}$ in relation to the others cases. The second device might generate the same energy than the first device in the worst cases. Comparing one device with the previous, the same situation happens for the other optimal cases. On the other hand, when robust cases (smallest resistances) for devices were considered the first device generate $(97.65 \pm 9.56) mW\ g^{-2}$ and is always the best. The second device might generate the same energy than the first device, but the probability is low and it decreased in relation to the deterministic case.

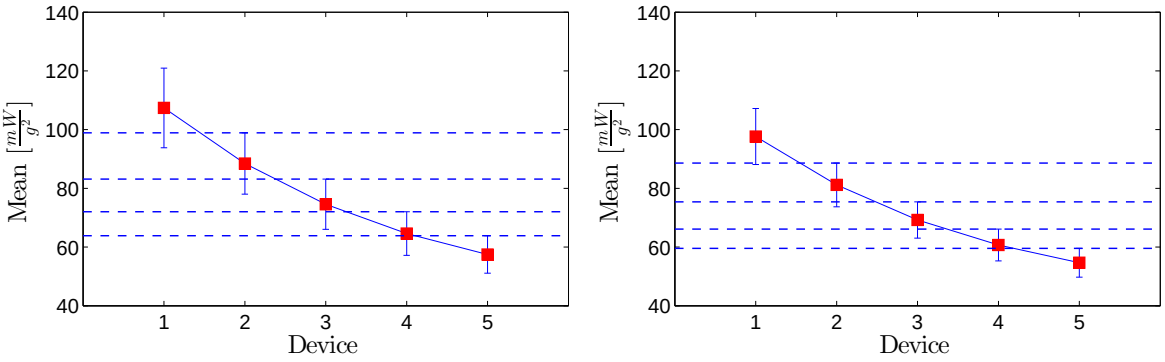

(a) Optimum Cases (b) Robust Cases

Figure 9. Mean values and 3σ confidence intervals for the power output of the five harvesting devices when using (a) best deterministic resistance and (b) more robust resistance.

6. CONCLUSION

This work presented recent results of robust design and uncertainty analysis of a resonant energy harvesting. This was done using a finite element model of a cantilever beam with tip mass and base excitation combined to deterministic and robust optimization using orthogonal arrays. Results indicate that the proposed methodology may help determining the best device design based not only on mean performance but also on robustness when subjected to uncertainties of clamp stiffness, damping and electrical resistance. It is shown that the device with larger mass, and smaller length, yields the better nominal harvesting performance but is also the less robust. On the other hand, electric resistances smaller than optimal ones may improve robustness with little reduction of mean performance.

7. ACKNOWLEDGEMENTS

Authors acknowledge financial support of MCT/CNPq/FAPEMIG National Institute of Science and Technology on Smart Structures in Engineering, grant 574001/2008-5, and CNPq research grants 134508/2015-7 and 309193/2014-1.

8. REFERENCES

Erturk, A. and Inman, D.J., 2011. *Piezoelectric energy harvesting*. John Wiley & Sons, New Jersey, 1st edition.

Kalyani, V.L., Piaus, A. and Vyas, P., 2015. "Harvesting electrical energy via vibration energy and its applications". *Journal of Management Engineering and Information Technology*, Vol. 2, pp. 9–14.

Leo, D.J., 2007. *Engineering analysis of smart material systems*. John Wiley & Sons, New Jersey.

Park, G.J., Lee, T.H., Lee, K.H. and Hwang, K.H., 2006. "Robust design: an overview". *AIAA journal*, Vol. 44, No. 1, pp. 181–191.

Phadke, M.S., 1995. *Quality engineering using robust design*. Prentice Hall PTR, New Jersey.

Ramadan, K.S., Sameoto, D. and Evoy, S., 2014. "A review of piezoelectric polymers as functional materials for electromechanical transducers". *Smart Materials and Structures*, Vol. 23, No. 3, p. 033001.

Rao, S.S., 2009. *Engineering optimization: theory and practice*. John Wiley & Sons, New Jersey.

Santos, H., 2008. *Structural vibration control using piezoceramics in extension and shear connected to hybrid active-passive circuits (in portuguese)*. Master's thesis, University of São Paulo.

Santos, H., 2012. *Active-passive structural control using piezoelectric materials: optimization and uncertainty quantification (in portuguese)*. Ph.D. thesis, University of São Paulo.

Schuëller, G.I. and Jensen, H.A., 2008. "Computational methods in optimization considering uncertainties–an overview". *Computer Methods in Applied Mechanics and Engineering*, Vol. 198, No. 1, pp. 2–13.

Trindade, M., Santos, H. and Godoy, T.C., 2013. "Effect of bonding layer uncertainties on the performance of surface-mounted piezoelectric sensors and actuators". In *Proceedings of the XIV International Symposium on Dynamic Problems of Mechanics - ABCM*. Buzios, Brazil.

Zang, C., Friswell, M. and Mottershead, J., 2005. "A review of robust optimal design and its application in dynamics". *Computers & structures*, Vol. 83, No. 4, pp. 315–326.

9. RESPONSIBILITY NOTICE

The authors are the only responsible for the printed material included in this paper.